ECCOMAS Congress 2016, Crete Island, Greece, 5-10 June 2016

Curved grid generation and DG computation for the DLR-F11 high lift configuration

Ralf Hartmann[1], Harlan McMorris[2], Tobias Leicht[1]

[1]DLR (German Aerospace Center), Institute of Aerodynamics and Flow Technology, Braunschweig

[2]CentaurSoft, Austin, TX

10. June 2016

HioCFD-4 Computational/Meshing Challenge DLR-F11

Meshing challenge:

- Quadratic hybrid/mixed-element meshes by the CENTAUR grid generator

Computational challenge:

- Stabilized DG discretization and implicit solver in the DLR-PADGE code

DLR-F11 high-lift configuration
with slat tracks and flap track fairings

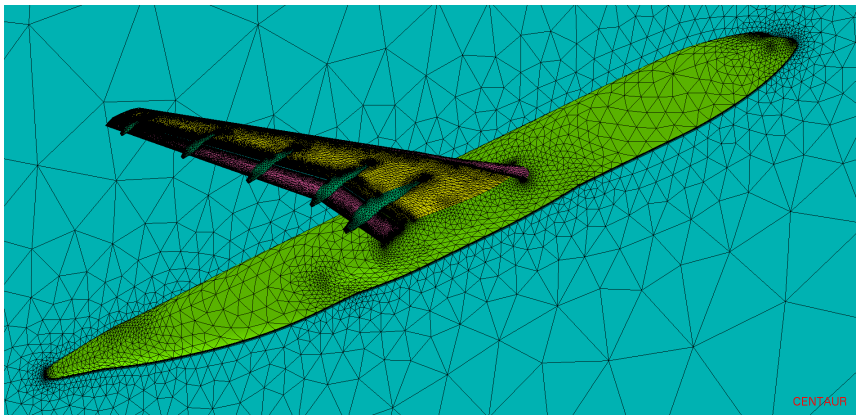

hybrid/mixed-element 3rd-order grid

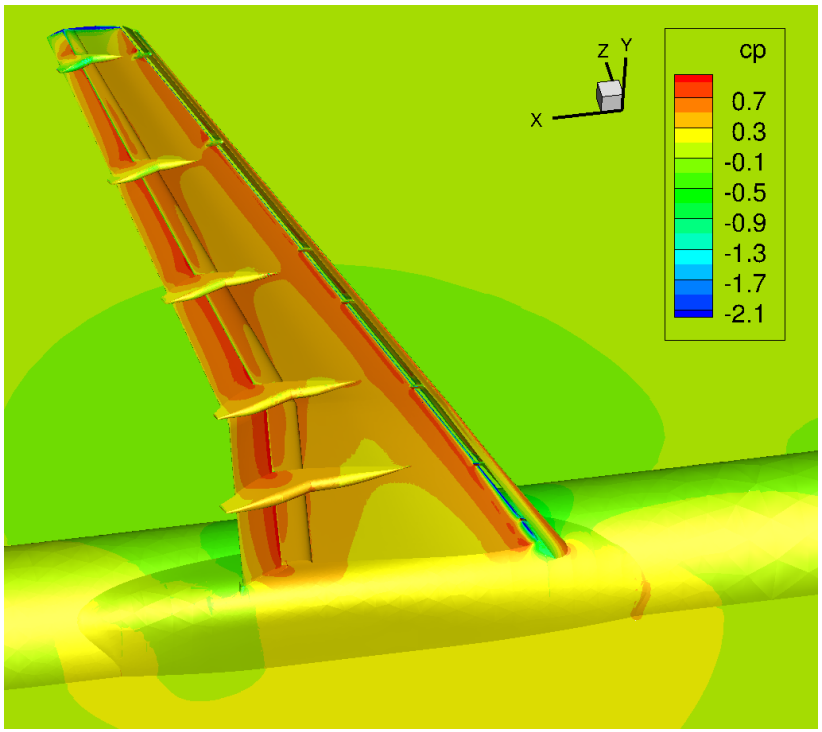

3rd-order flow solution

Linear and quadratic mesh generation process (CENTAUR)

(1) Generate a coarse, linear hybrid grid.

(2) Insert an additional midpoint for every grid edge and quadrilateral face.

(3) Use the CAD information to map each new boundary point onto the underlying CAD surface.

(4) Adjust the position of the interior points based on the mapped position of the boundary edge midpoints, in order to prevent self-intersecting grid elements and to ensure grid validity.

(5) Quadratic interpolation of points and interior points for a curved element representation.

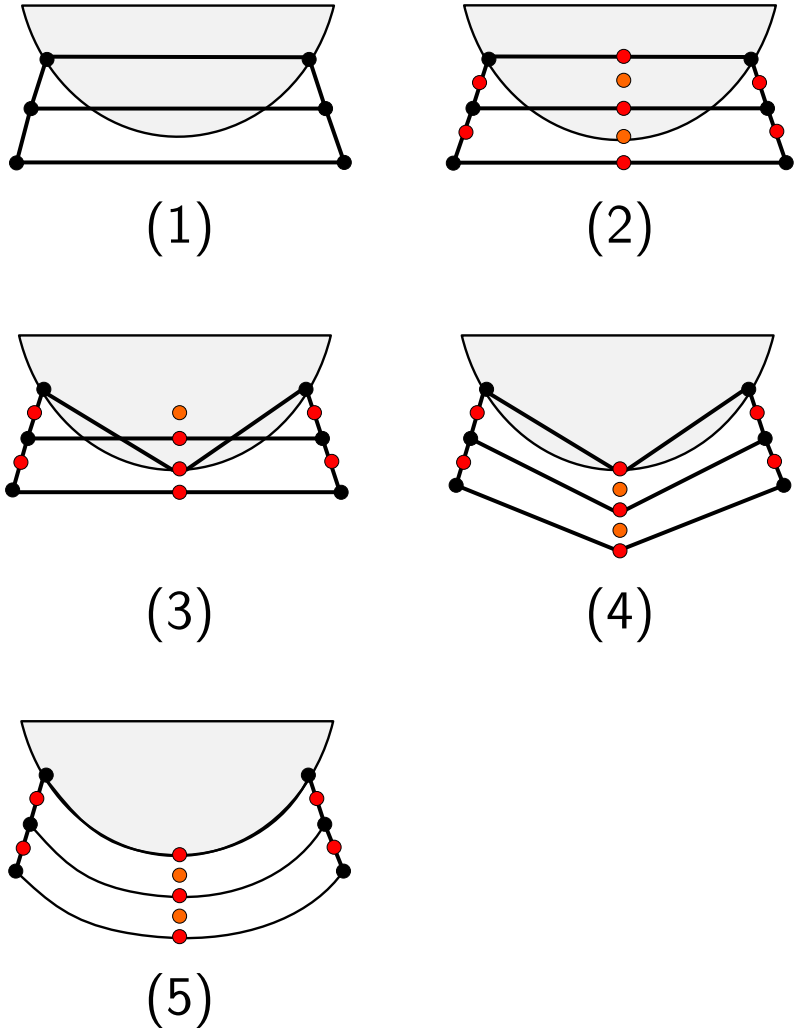

Linear and quadratic mesh generation process (CENTAUR)

For the grid generation of a particularly coarse linear mesh

- a lower analytic curvature clustering, and
- a larger maximum element size

are used than for linear meshes typically generated for 2nd order schemes.

After curving of the mesh the grid quality is evaluated using

- the volumes, and the
- the volume ratios

of the complete elements and sub-elements.

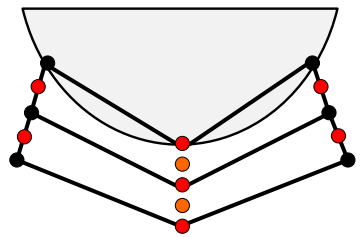

Linear and quadratic mesh generation process: Examples

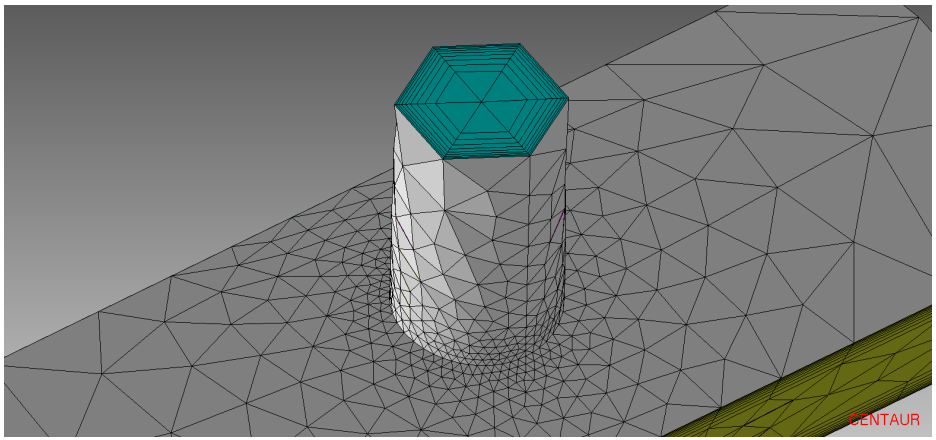

linear mesh

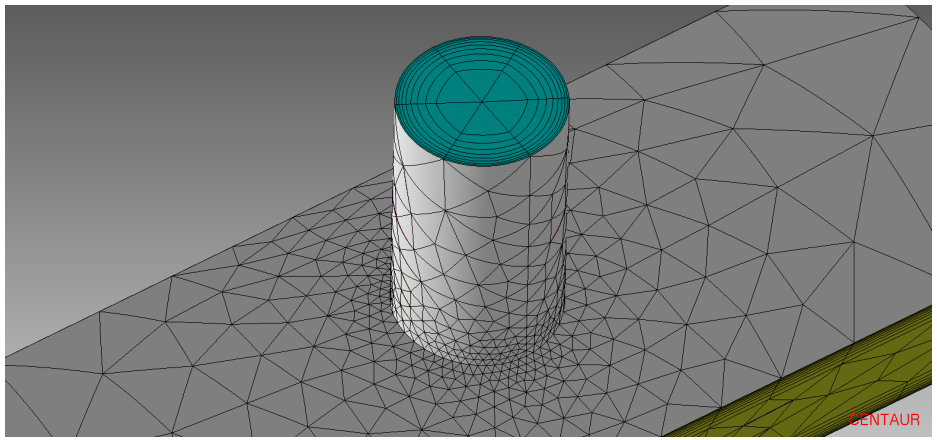

quadratic mesh

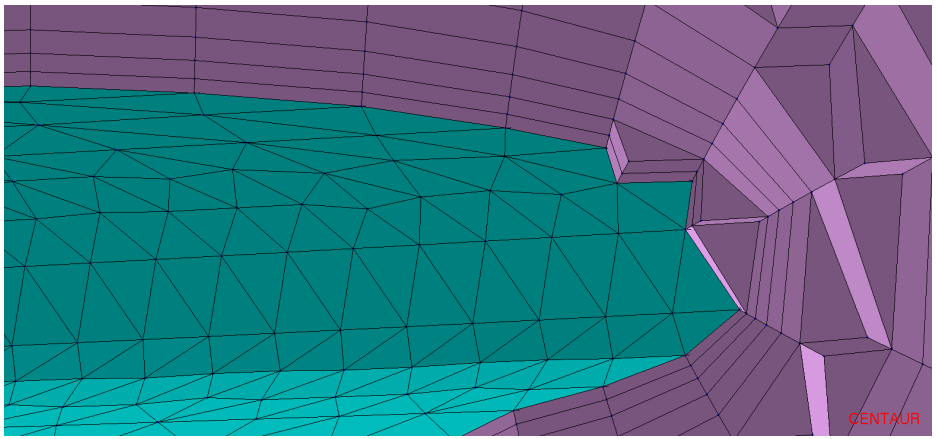

linear mesh

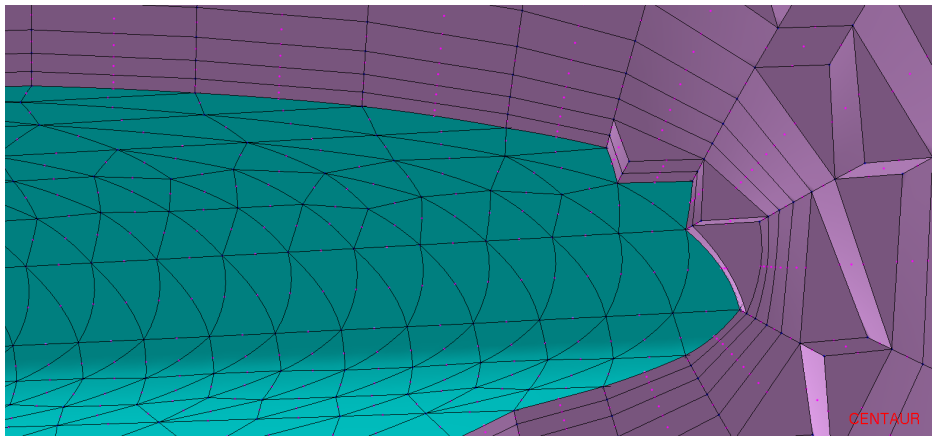

quadratic mesh

Linear and quadratic mesh generation: Application to DLR-F11

Coarse mesh with

2 365 919	prisms
42 603	pyramids
1 116 213	tetrahedra
3 524 735	elements

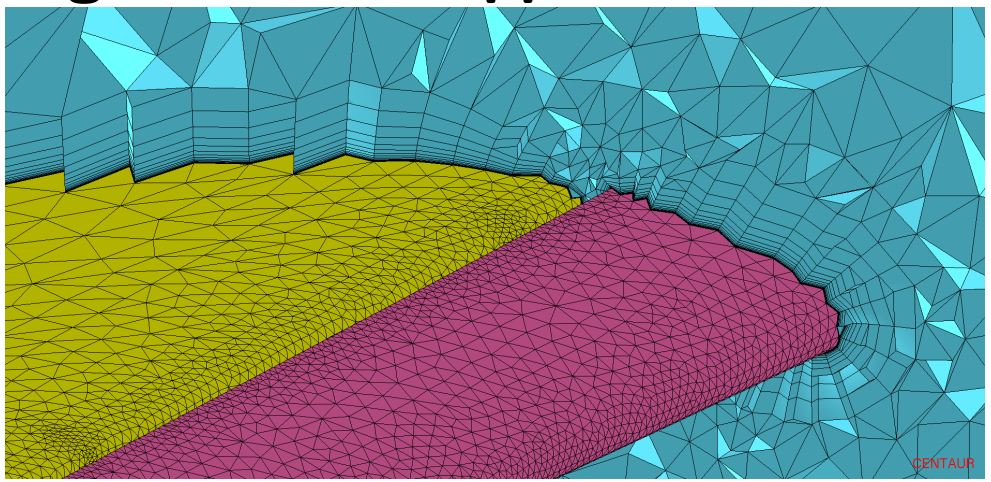

prism layers around the slat and leading edge of the main

Outboard flap track fairing surface mesh:

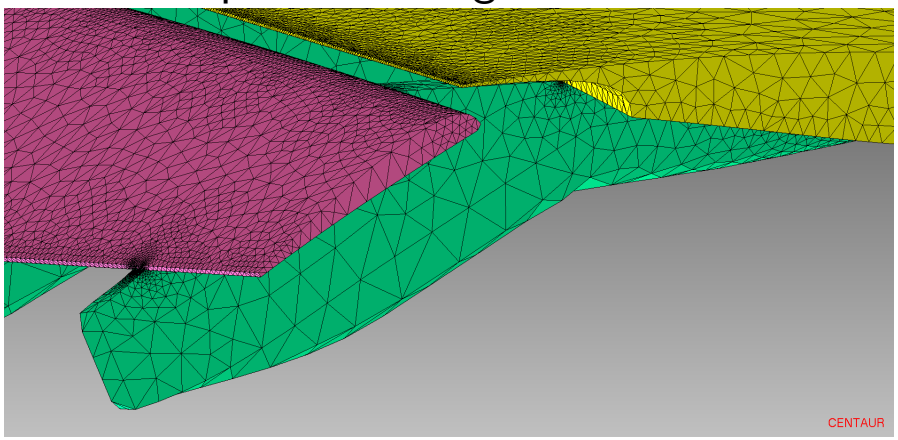

linear mesh

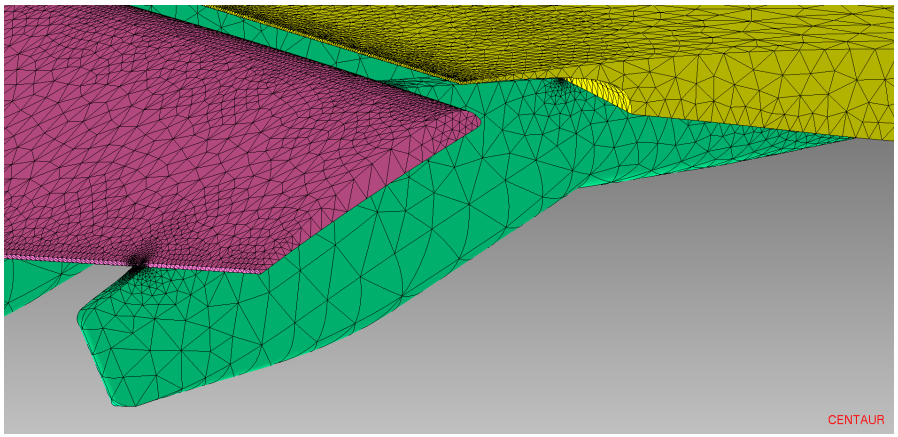

quadratic mesh

Linear and quadratic mesh generation: Application to DLR-F11

Coarse mesh with

2 365 919	prisms
42 603	pyramids
1 116 213	tetrahedra
3 524 735	elements

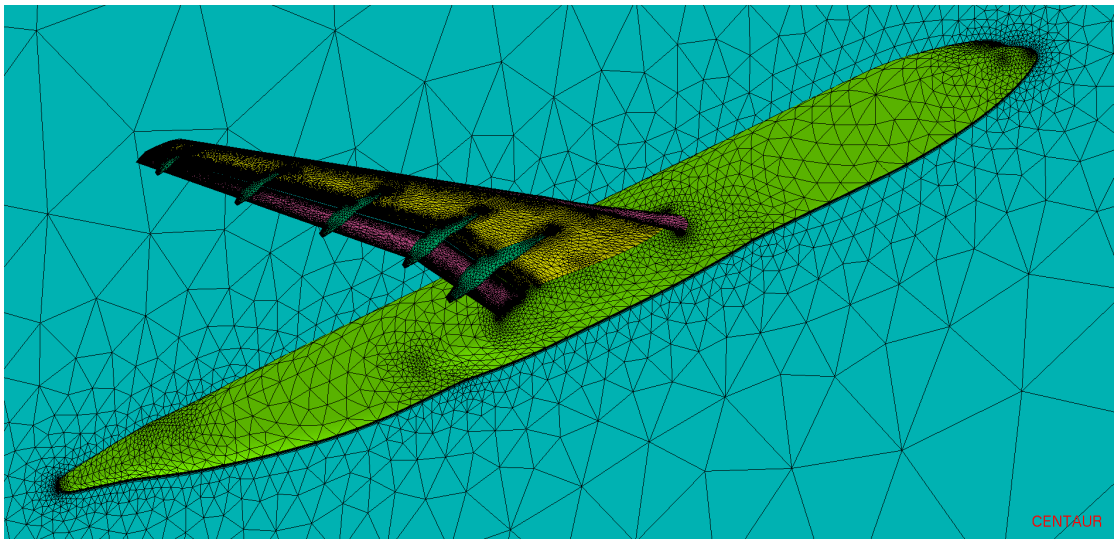

Hybrid mesh cuts in the slat region:

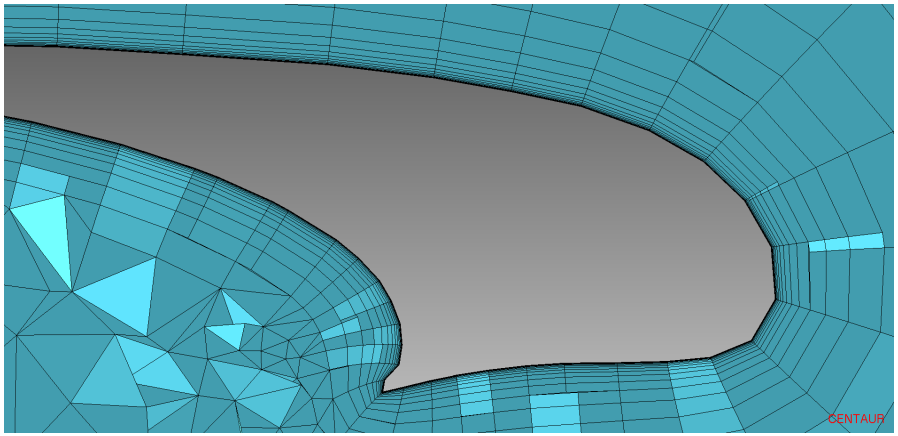

linear mesh

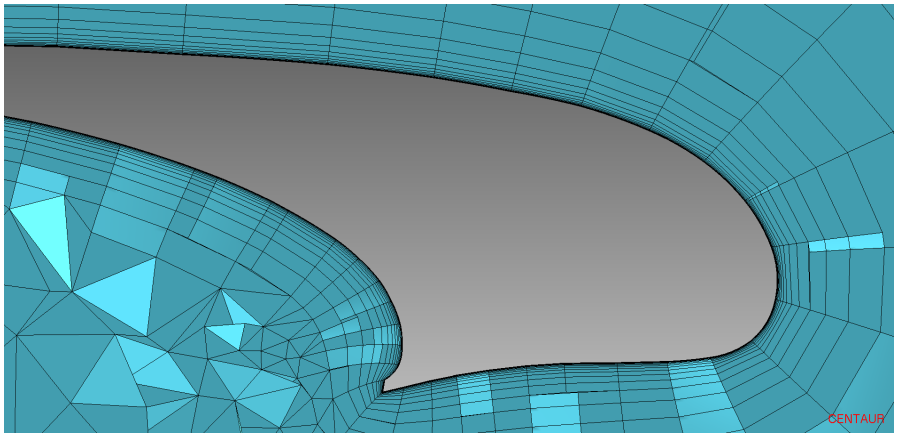

quadratic mesh

The DG discretization of the compressible Euler equations

The problem:

$$\nabla \cdot \mathcal{F}^c(\mathbf{u}) = 0 \quad \text{in } \Omega \subset \mathbb{R}^2,$$

with $\mathbf{u} = (\varrho, \varrho v_1, \varrho v_2, \varrho E)^T$.

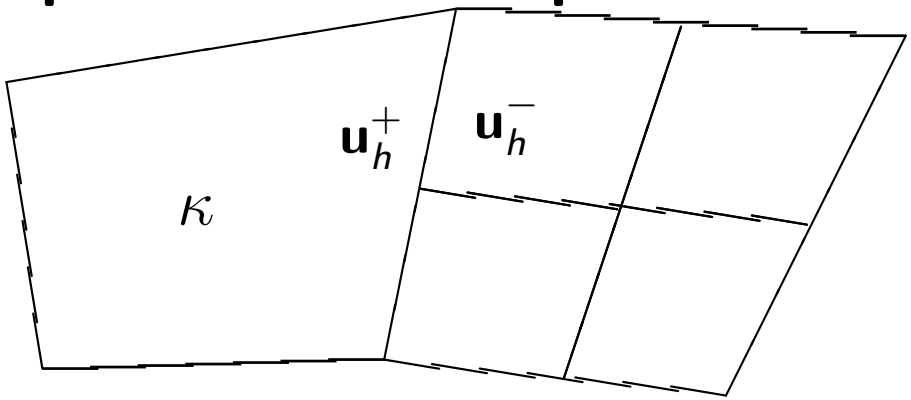

The DG(p) discretization: Find $\mathbf{u}_h$ in $\mathbf{V}_h^p$ such that

$$N_h(\mathbf{u}_h, \mathbf{v}_h) \equiv \sum_{\kappa \in \mathcal{T}_h} \left\{ -\int_\kappa \mathcal{F}^c(\mathbf{u}_h) : \nabla \mathbf{v}_h \, \mathrm{d}\mathbf{x} + \int_{\partial\kappa \setminus \Gamma} \hat{\mathbf{h}}(\mathbf{u}_h^+, \mathbf{u}_h^-, \mathbf{n}) \cdot \mathbf{v}_h^+ \, \mathrm{d}s \right\}$$
$$+ \int_\Gamma \hat{\mathbf{h}}_\Gamma(\mathbf{u}_h^+, \mathbf{n}) \cdot \mathbf{v}_h^+ \, \mathrm{d}s = 0 \quad \forall \mathbf{v}_h \in \mathbf{V}_h^p,$$

Numerical flux function $\hat{\mathbf{h}}$: Roe flux, local Lax-Friedrichs flux, ...
Numerical flux function $\hat{\mathbf{h}}_\Gamma$ at the boundary:

- $\hat{\mathbf{h}}_\Gamma(\mathbf{u}_h^+, \mathbf{n}) = \mathbf{n} \cdot \mathcal{F}^c(\mathbf{u}_\Gamma(\mathbf{u}_h^+))$ allows for an adjoint consistent discretization
- $\hat{\mathbf{h}}_\Gamma(\mathbf{u}_h^+, \mathbf{n}) = \hat{\mathbf{h}}(\mathbf{u}_h^+, \mathbf{u}_\Gamma^\star(\mathbf{u}_h^+), \mathbf{n})$ is, to our experience, significantly more stable

Numerical flux function at the boundary

Use the same numerical flux on the boundary like on interior faces

$$\hat{\mathbf{h}}_{\Gamma,h} = \hat{\mathbf{h}}_{\Gamma}(\mathbf{u}_h^+, \mathbf{n}) = \hat{\mathbf{h}}(\mathbf{u}_h^+, \mathbf{u}_{\Gamma}^-(\mathbf{u}_h^+), \mathbf{n}),$$

where the *boundary exterior state* $\mathbf{u}_{\Gamma}^-(\mathbf{u}_h^+)$ is computed from $\frac{1}{2}\left(\mathbf{u}_h^+ + \mathbf{u}_{\Gamma}^-(\mathbf{u}_h^+)\right) = \mathbf{u}_{\Gamma}(\mathbf{u}_h^+)$ with $\mathbf{n} \cdot \mathbf{v}_{\Gamma} = 0$, the discretization is given by

$$-\int_{\Omega} \mathcal{F}^c(\mathbf{u}_h) : \nabla_h \mathbf{v}_h \, \mathrm{d}\mathbf{x} + \sum_{\kappa \in \mathcal{T}_h} \int_{\partial\kappa \setminus \Gamma} \hat{\mathbf{h}}_h \cdot \mathbf{v}_h^+ \, \mathrm{d}s + \int_{\Gamma} \hat{\mathbf{h}}(\mathbf{u}_h^+, \mathbf{u}_{\Gamma}^-(\mathbf{u}_h^+), \mathbf{n}) \cdot \mathbf{v}_h^+ \, \mathrm{d}s = 0.$$

This discretization is **adjoint inconsistent** in combination with both

$$J_h(\mathbf{u}_h) = \int_{\Gamma_W} p\left(\mathbf{u}_{\Gamma}(\mathbf{u}_h^+)\right) \, \mathbf{n} \cdot \boldsymbol{\psi} \, \mathrm{d}s = J(\mathbf{u}_{\Gamma}(\mathbf{u}_h^+)),$$

and

$$J(\mathbf{u}_h) = \int_{\Gamma_W} p(\mathbf{u}_h) \, \mathbf{n} \cdot \boldsymbol{\psi} \, \mathrm{d}s.$$

Adjoint consistent discretization of force coefficients

Consider the discretization: find $\mathbf{u}_h$ in $\mathbf{V}_h^p$ such that

$$-\int_\Omega \mathcal{F}^c(\mathbf{u}_h) : \nabla \mathbf{v}_h \, \mathrm{d}\mathbf{x} + \sum_{\kappa \in \mathcal{T}_h} \int_{\partial\kappa \setminus \Gamma} \hat{\mathbf{h}}_h \cdot \mathbf{v}_h^+ \, \mathrm{d}s + \int_\Gamma \hat{\mathbf{h}}_{\Gamma,h} \cdot \mathbf{v}_h^+ \, \mathrm{d}s = 0 \quad \mathbf{v}_h \in \mathbf{V}_h^p \tag{1}$$

Consider the target quantity and its discretization

$$J(\mathbf{u}) = \int_{\Gamma_W} p(\mathbf{u})\, \mathbf{n} \cdot \boldsymbol{\psi} \, \mathrm{d}s, \qquad J_h(\mathbf{u}_h) = \int_{\Gamma_W} \hat{\mathbf{h}}_{\Gamma,h} \cdot \tilde{\boldsymbol{\psi}} \, \mathrm{d}s, \tag{2}$$

with $\tilde{\boldsymbol{\psi}} = (0, \psi_1, \psi_2, 0)^\top$ for $\boldsymbol{\psi} = (\psi_1, \psi_2)^\top$, and

$$\hat{\mathbf{h}}_{\Gamma,h} = \hat{\mathbf{h}}_\Gamma(\mathbf{u}_h^+, \mathbf{n}) = \hat{\mathbf{h}}(\mathbf{u}_h^+, \mathbf{u}_\Gamma^-(\mathbf{u}_h^+), \mathbf{n}),$$

It can be shown[1], that (1) in combination with (2) is **adjoint consistent**.

[1] R. Hartmann and T. Leicht. Generalized adjoint consistent treatment of wall boundary conditions for compressible flows, J. Comput. Phys., 300: 754-778, 2015.

Example: Inviscid flow around the NACA0012 airfoil

$M = 0.5$, $\alpha = 2°$, numerical flux at the wall boundary: $\hat{\mathbf{h}}_{\Gamma,h} = \hat{\mathbf{h}}(\mathbf{u}_h^+, \mathbf{u}_\Gamma^-(\mathbf{u}_h^+), \mathbf{n})$

z_1 isolines of the discrete adjoint solution $\mathbf{z}_h$ for C_{dp}:

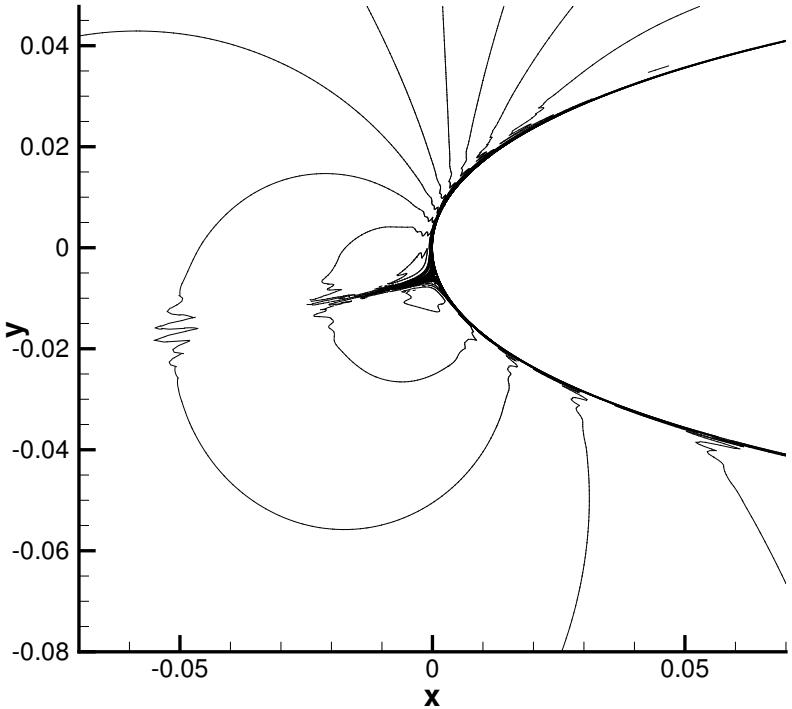

$J_h(\mathbf{u}_h) = J(\mathbf{u}_\Gamma(\mathbf{u}_h^+))$

adjoint inconsistent

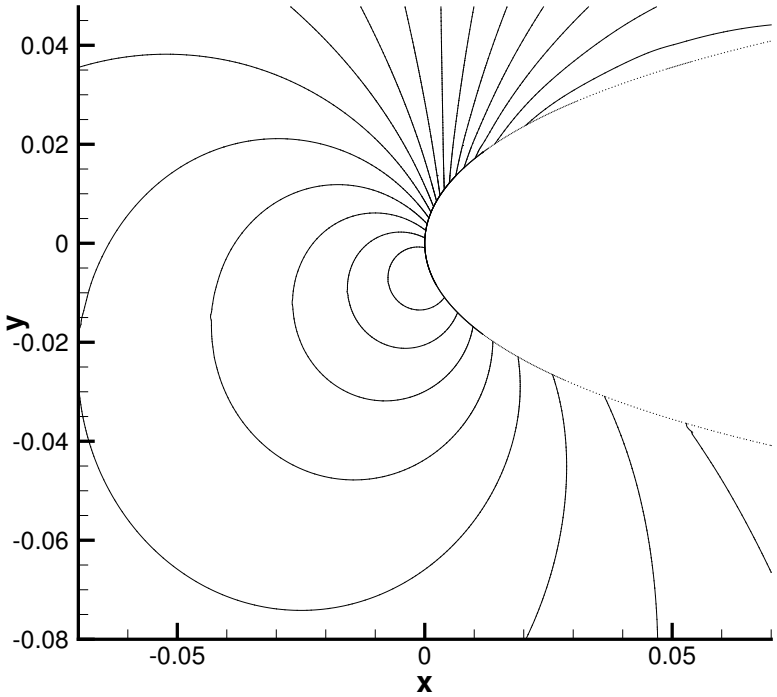

$J_h(\mathbf{u}_h) = \int_{\Gamma_W} \hat{\mathbf{h}}_{\Gamma,h} \cdot \tilde{\psi} \, \mathrm{d}s$

adjoint consistent

Extension to viscous flows

$$\int_\Omega \left(-\mathcal{F}^c(\mathbf{u}_h) + \mathcal{F}^v(\mathbf{u}_h, \nabla_h \mathbf{u}_h)\right) \,:\, \nabla_h \mathbf{v}_h \,\mathrm{d}\mathbf{x} + \ldots + \int_\Gamma \left(\hat{\mathbf{h}}_{\Gamma,h} - \underline{\hat{\sigma}}_{\Gamma,h}\mathbf{n}\right) \cdot \mathbf{v}_h \,\mathrm{d}s$$

is **adjoint consistent** in combination with

$$J(\mathbf{u}) = \int_{\Gamma_w} (p\,\mathbf{n} - \underline{\tau}\,\mathbf{n}) \cdot \boldsymbol{\psi} \,\mathrm{d}s, \qquad J_h(\mathbf{u}_h) = \int_{\Gamma_w} \left(\hat{\mathbf{h}}_{\Gamma,h} - \underline{\hat{\sigma}}_{\Gamma,h}\mathbf{n}\right) \cdot \tilde{\boldsymbol{\psi}} \,\mathrm{d}s,$$

with $\tilde{\boldsymbol{\psi}} = (0, \psi_1, \psi_2, 0)^\top$ for $\boldsymbol{\psi} = (\psi_1, \psi_2)^\top$.

Adjoint consistent treatment of integral and local quantities

Discretization of flow equations:

$$\int_\Omega \left(-\mathcal{F}^c(\mathbf{u}_h) + \mathcal{F}^v(\mathbf{u}_h, \nabla_h \mathbf{u}_h)\right) \,:\, \nabla_h \mathbf{v}_h \,\mathrm{d}\mathbf{x} + \ldots + \int_\Gamma \left(\hat{\mathbf{h}}_{\Gamma,h} - \underline{\hat{\sigma}}_{\Gamma,h}\mathbf{n}\right) \cdot \mathbf{v}_h \,\mathrm{d}s$$

Adjoint consistent discretization of **integral** quantities (drag, lift coefficients):

$$J(\mathbf{u}) = \int_{\Gamma_W} (p\,\mathbf{n} - \underline{\tau}\,\mathbf{n}) \cdot \boldsymbol{\psi} \,\mathrm{d}s, \qquad J_h(\mathbf{u}_h) = \int_{\Gamma_W} \left(\hat{\mathbf{h}}_{\Gamma,h} - \underline{\hat{\sigma}}_{\Gamma,h}\mathbf{n}\right) \cdot \tilde{\boldsymbol{\psi}} \,\mathrm{d}s.$$

Adjoint consistent discretization of **local** quantities (surface pressure, skin friction):

$$c_\mathrm{p}(\mathbf{u}) = \frac{p(\mathbf{u}) - p_\infty}{\frac{1}{2}\rho_\infty v_\infty^2}, \qquad c_{\mathrm{p},h}(\mathbf{u}_h) = \frac{\hat{\mathbf{h}}_{\Gamma,h} \cdot \tilde{\mathbf{n}} - p_\infty}{\frac{1}{2}\rho_\infty v_\infty^2},$$

$$c_\mathrm{f}(\mathbf{u}, \nabla\mathbf{u}) = \frac{\tau_W(\mathbf{u}, \nabla\mathbf{u})}{\frac{1}{2}\rho_\infty v_\infty^2}, \qquad c_{\mathrm{f},h}(\mathbf{u}_h, \nabla\mathbf{u}_h) = -\frac{\left(\underline{\hat{\sigma}}_{\Gamma,h}\mathbf{n}\right) \cdot \tilde{\mathbf{t}}}{\frac{1}{2}\rho_\infty v_\infty^2},$$

with $\tilde{\mathbf{n}} = (0, n_1, n_2, 0)^\top$ for the normal vector $\mathbf{n} = (n_1, n_2)^\top$,
and $\tilde{\mathbf{t}} = (0, t_1, t_2, 0)^\top$ for the tangential vector $\mathbf{t} = (t_1, t_2)^\top$.

Example: L1T2 high-lift configuration

RANS & Wilcox k-ω model, $M = 0.197$, $\alpha = 20.18°$, $Re = 3.52 \times 10^6$

$$\hat{\mathbf{h}}_{\Gamma,h} = \hat{\mathbf{h}}_{\Gamma}(\mathbf{u}_h^+, \mathbf{n}) = \hat{\mathbf{h}}(\mathbf{u}_h^+, \mathbf{u}_{\Gamma}^-(\mathbf{u}_h^+), \mathbf{n}).$$

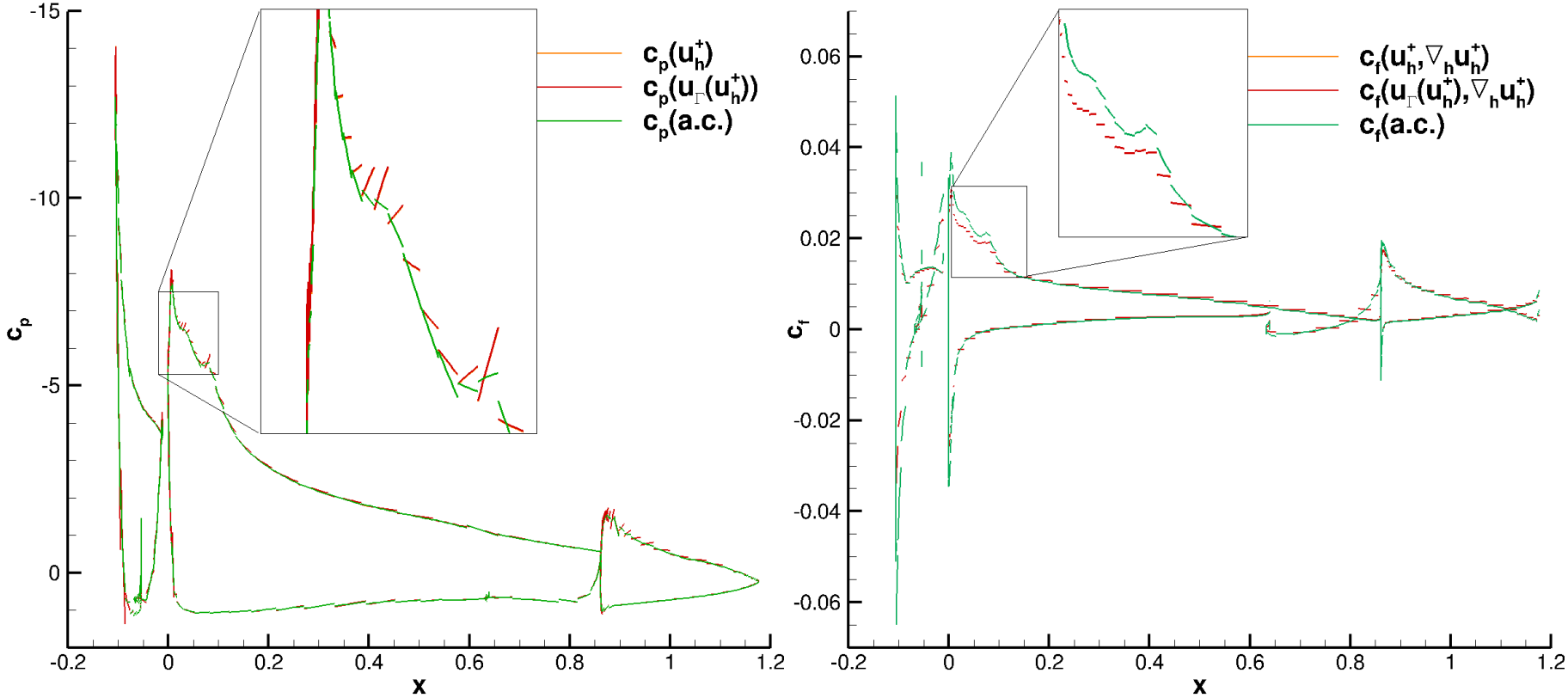

c_p- and c_f-distributions of the $p = 1$ flow solution

Regularity check of a curved mesh

Discrete regularity check:

- Consider the mapping σ from the reference element $\hat{\kappa}$ to the element κ in physical space. The determinant of its Jacobian matrix $\frac{d\sigma}{d\mathbf{x}}$ is required in numerical quadrature:

$$|\kappa| = \int_{\hat{\kappa}} \det(J)\, \mathrm{d}\mathbf{x} \approx \sum_q \det(J(\hat{\mathbf{x}}_q)) w_q$$

- Check whether the Jacobian determinants $\det(J(\hat{\mathbf{x}}_q))$ are positive in each of the quadrature points.

Note,

- that this discrete regularity check checks *necessary* conditions only,
- whereas the check based on Bézier functions[1] would give a *necessary and sufficient* condition for validity.

[1] A. Johnen, J.-F. Remacle, and C. Geuzaine. Geometrical validity of curvilinear finite elements. *J. Comput. Phys.*, 233:359–272, 2013.

Regularity check of the quadratic DLR-F11 mesh

$$|\kappa| = \int_{\hat{\kappa}} \det(J)\, \mathrm{d}\mathbf{x} \approx \sum_q \det(J(\mathbf{x_q}))\, w_q$$

Discrete regularity check: $\det(J(\mathbf{x_q})) > 0$ for all quadrature points $\mathbf{x}_q$?

"Discrete regularity" check of the quadratic mesh around the DLR-F11 mesh with 3 524 735 curved elements (prisms, pyramids and tetrahedras):

degree	# DoFs/eqn	# quadrature points/elem.	# irregular elements	worst # neg. Jac./element
0	3 524 735	8	0	0/8
1	14 098 940	27	0	0/27
2	35 247 350	64	14	2/64

Application to the DLR-F11 (Config 4): The solution process

RANS & Wilcox k-ω model, flow conditions: $M = 0.175$, $Re = 15.1 \cdot 10^6$, $\alpha = 7°$
Flow solver:

- Fully implicit (Backward-Euler) solver
- Convergence criterion: nonlinear residual below 10^{-10}.
- Linear systems solved with GMRes and ILU per process
- The CFL number is increased as the nonlinear residual decreases
- Diverging steps are recomputed with CFL/2.

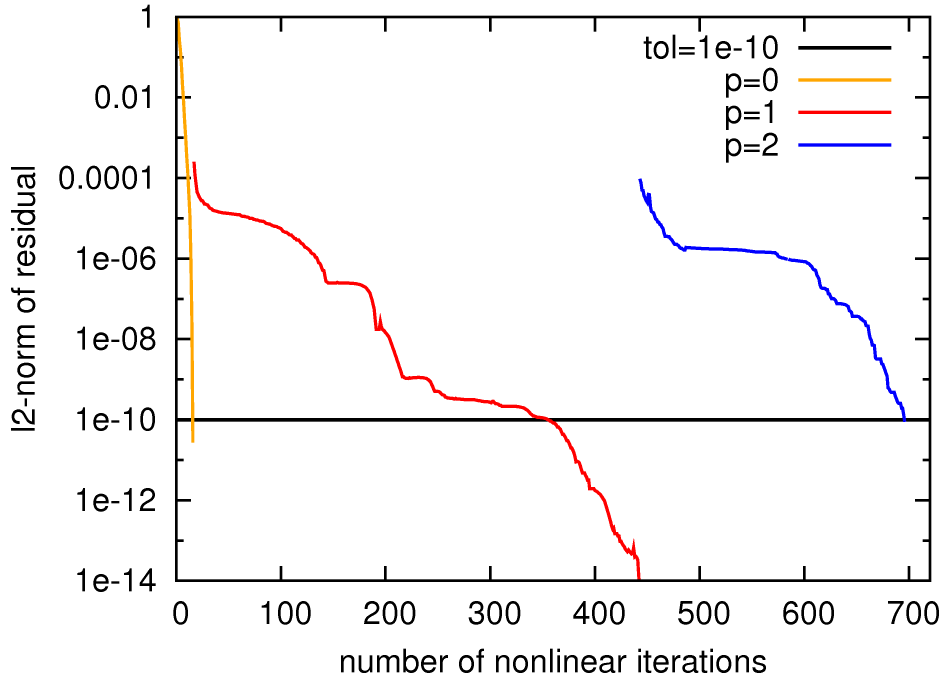

Numerical boundary flux: $\hat{\mathbf{h}}_\Gamma = \hat{\mathbf{h}}(\mathbf{u}_h^+, \mathbf{u}_\Gamma^-(\mathbf{u}_h^+), \mathbf{n})$.

degree	# DoFs/eqn	res tol	start CFL	end CFL	steps lost
0	3.5e6	10^{-10}	100	120 000	0/16
1	14.1e6	10^{-10}	5	500	45/339
		$\ldots 10^{-14}$	500	40 000	+18/87
2	35.2e6	10^{-10}	10	200	24/254

Application to the DLR-F11 (Config 4): The solution process

RANS & Wilcox k-ω model, flow conditions: $M = 0.175$, $Re = 15.1 \cdot 10^6$, $\alpha = 7°$
Flow solver:

- Fully implicit (Backward-Euler) solver
- Convergence criterion: nonlinear residual below 10^{-10}.
- Linear systems solved with GMRes and ILU per process
- The CFL number is increased as the nonlinear residual decreases

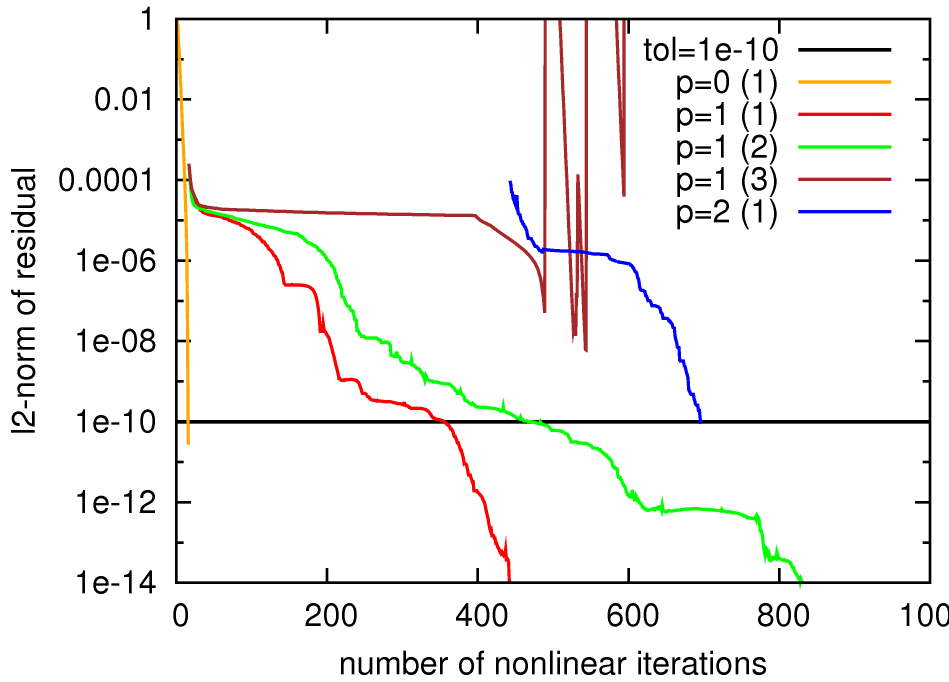

legend	numerical flux	recompute diverging steps with CFL/2
p=1 (1)	$\hat{\mathbf{h}}(\mathbf{u}_h^+, \mathbf{u}_\Gamma^-(\mathbf{u}_h^+), \mathbf{n})$	yes
p=1 (2)	$\mathbf{n} \cdot \mathcal{F}^c(\mathbf{u}_\Gamma(\mathbf{u}_h^+))$	yes
p=1 (3)	$\mathbf{n} \cdot \mathcal{F}^c(\mathbf{u}_\Gamma(\mathbf{u}_h^+))$	no

DLR-F11 high lift configuration: The flow solution

RANS & Wilcox k-ω model, flow conditions: $M = 0.175$, $Re = 15.1 \cdot 10^6$, $\alpha = 7°$.
3^{rd}-order solution on the quadratic (3^{rd}-order) mesh:

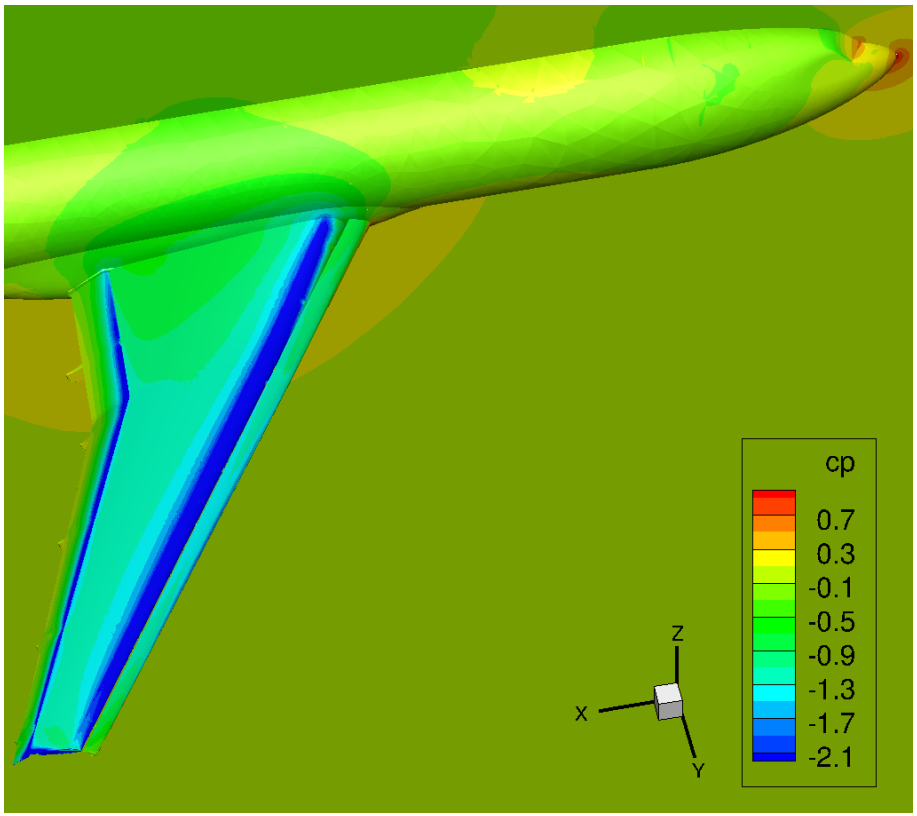

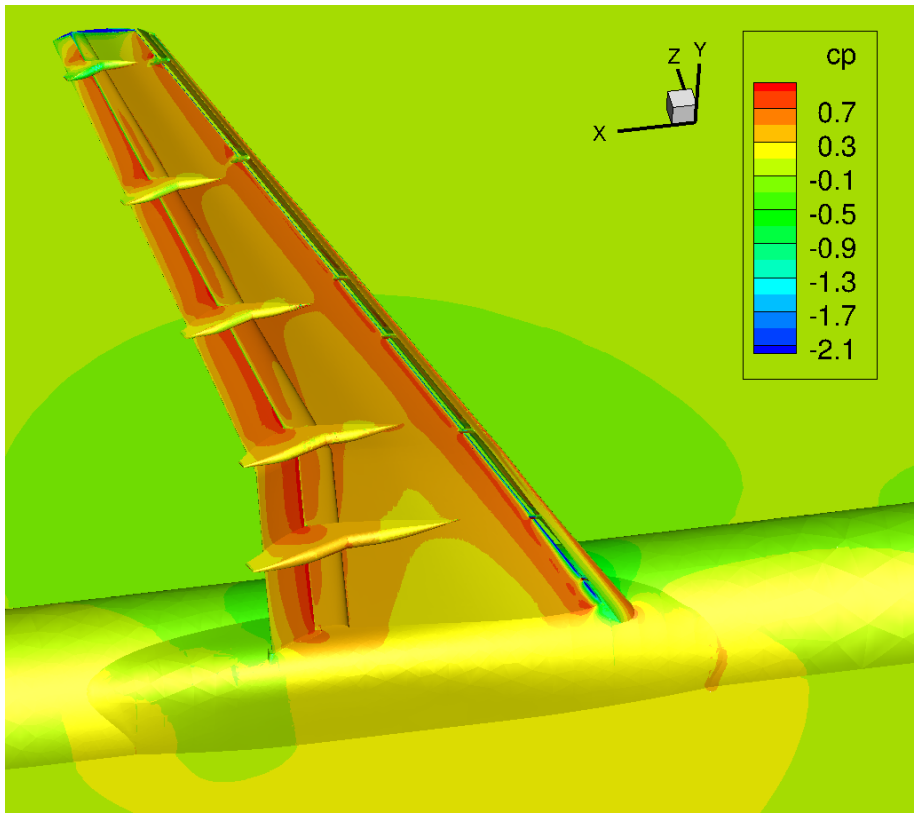

DLR-F11 high lift configuration: The flow solution

RANS & Wilcox k-ω model, flow conditions: $M = 0.175$, $Re = 15.1 \cdot 10^6$, $\alpha = 7°$.
3rd-order solution on the quadratic (3rd-order) mesh:

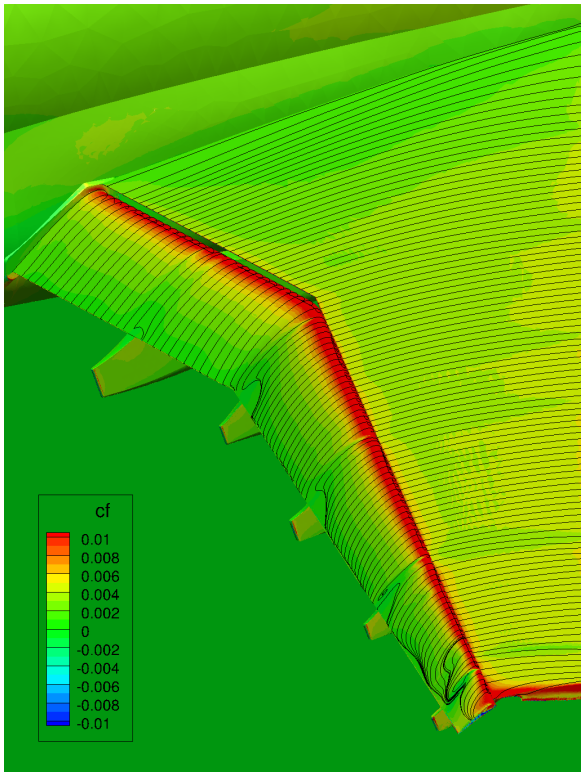

separation above flap track fairings and at wing tip

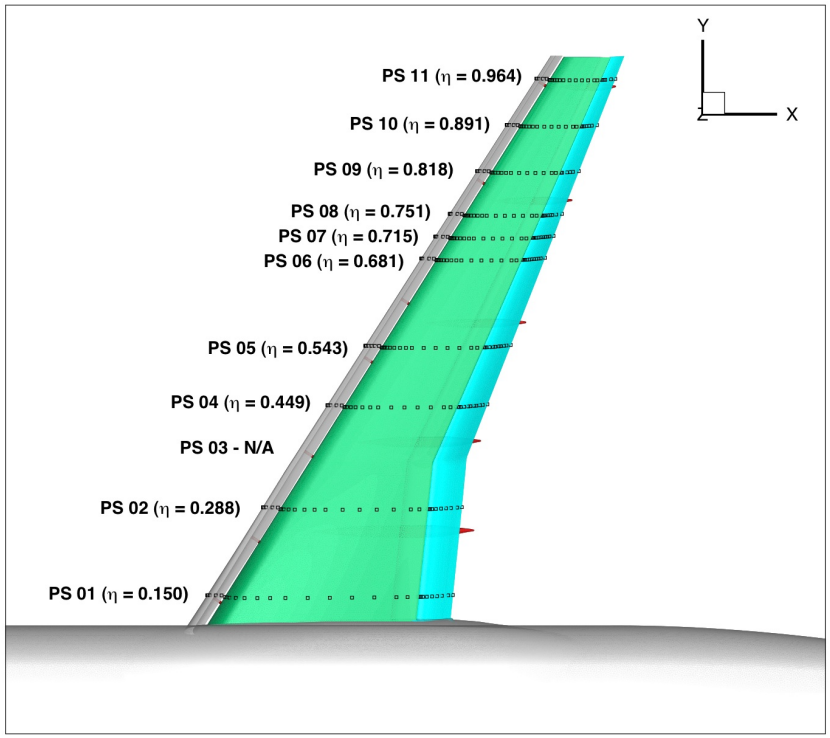

consider pressure tab locations 01, 04, 06, 10

DLR-F11 high lift configuration: The flow solution

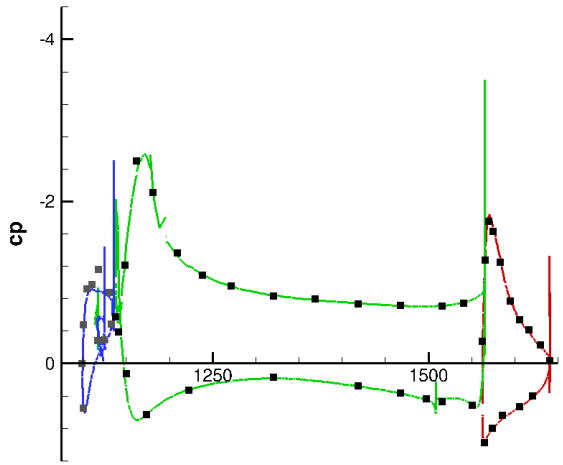

PS01(η=0.150)

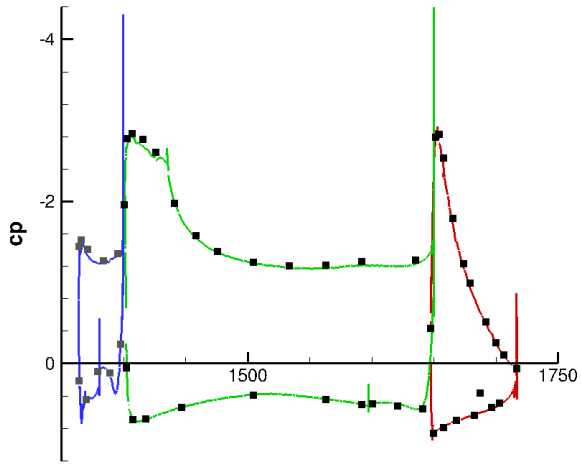

PS04(η=0.449)

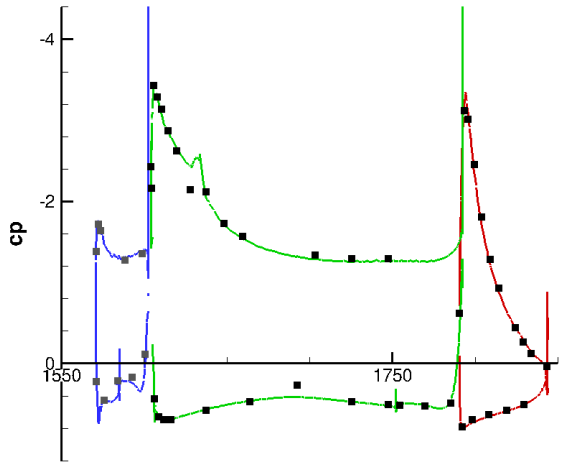

PS06(η=0.681)

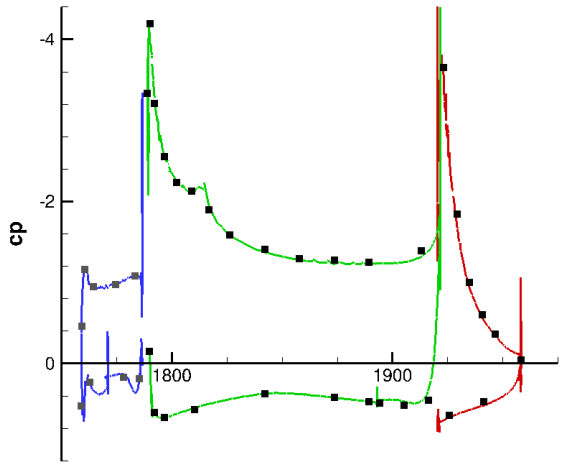

PS10(η=0.891)

RANS & Wilcox k-ω model

$M = 0.175$

$Re = 15.1 \cdot 10^6$

$\alpha = 7°$

3rd-order solution on 3rd-order mesh

	C_L	C_D	C_M
Exp.	1.927	0.162	-0.539
TAU	1.879	0.168	-0.565
	-2.5%	+4.1%	-4.8%
DG-O3	1.878	0.165	-0.570
	-2.5%	+2.1%	-5.8%

Computational/Meshing Challenge DLR-F11: Summary

- Quadratic hybrid/mixed-element mesh by the CENTAUR grid generator.
- Stabilized DG discretization and solver in the DLR-PADGE code:
  - For stability use interior flux also on the boundary. For adjoint consistency use the same flux also
    - for the evaluation of integral quantities (force coefficients), and
    - for an according evaluation of local quantities (c_p- and c_f-distributions)
  - Recompute diverging solver steps with CFL/2.

DLR-F11 high-lift configuration

with slat tracks and flap track fairings

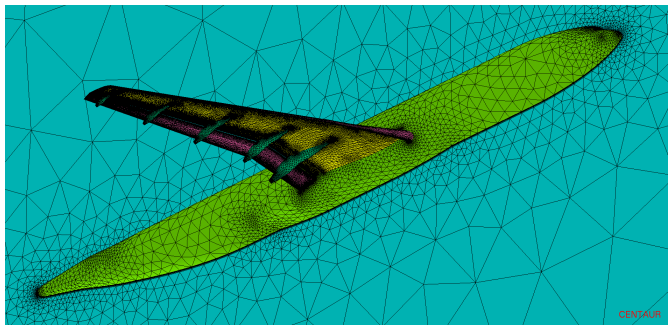

hybrid/mixed-element 3rd-order grid

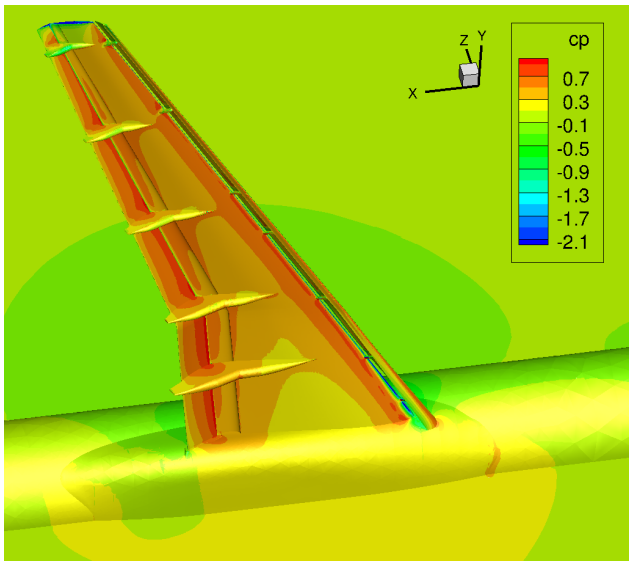

3rd-order flow solution